Journal of Power Sources 202 (2012) 357–363

Contents lists available at SciVerse ScienceDirect

Journal of Power Sources

journal homepage: www.elsevier.com/locate/jpowsour

Short communication

Microstructural and electrochemical investigation of functional nanostructured TiO_2 anode for Li-ions batteries

Alessandra Maria Serventi[a], Isadora Reis Rodrigues[a], Michel L. Trudeau[a], David Antonelli[b], Karim Zaghib[a,*]

[a] Institut de Recherche d'Hydro Québec, Expertise Science de Matériaux, Varennes, Québec, Canada J3X 1S1
[b] Sustainable Environment Research Center, University of Glamorgan, Pontypridd CF37-1DL, United Kingdom

ARTICLE INFO

Article history:
Received 19 September 2011
Received in revised form 9 November 2011
Accepted 10 November 2011
Available online 2 December 2011

Keywords:
Nanostructured TiO_2
Mesoporous
Anode
Li-ion battery
Carbon coating

ABSTRACT

We developed mesoporous and nanostructured TiO_2 anodes with very high specific surface, up to more than 500 $m^2 g^{-1}$, that show good promise for lithium battery applications. Modifying the surfactant to form a carbon coating inside the pores at low temperature shows better promises than normal carbonization processes, since the high temperature needed is too high and results in the crystal formation and the loss of porosity.

1. Introduction

Nanostructured materials show improved performances with respect to those of coarse-grained conventional ones in different fields of the material science. They present special physical, chemical and mechanical properties because of their high surface-to-volume ratio due to the enhanced density of interfaces and specific surface area [1–3].

TiO_2 is one of the most studied semiconductor oxides because of its versatility in energy and sensor applications. It is widely used in photo catalysis, lithium-ion batteries and dye sensitized solar cells [4–7]. Nanostructured TiO_2 has shown very good promises as anode materials in lithium-ion batteries because of its large capacity, high safety and fast ionic transport especially in nanostructured form.

Anatase is a fast Li insertion/extraction host with a high theoretical capacity around 336 mAh g^{-1} ($LiTiO_2$ for Ti^{3+}) with an appropriate insertion potential (~2.0 V) and a low volume expansion (3–4%) during insertion [8]. But practically about 0.5 Li at 1.78 V vs. Li/Li^+ (i.e. 168 mAh g^{-1}) can be reversibly inserted [9].

The presence of a fine porosity in the nanostructure highly influences the ionic transport and the volumetric capacity of electrodes because of a further increase of the specific surface area [10–14]. However, its cycling performance tends to be poor because of the aggregation of TiO_2 nanoparticles during cycling. In order to suppress this aggregation, researchers have attempted to disperse the nanoparticles into some carbon matrix or synthesize TiO_2—C core/shell structured nanocomposites [15].

Synthesis of mesoporous metal oxides and especially of mesoporous titanium oxide improves the potentiality of this material in all fields of applications [16–19]. In the last two decades numerous synthetic methods have been investigated and used to produce mesoporous TiO_2, such as hydrothermal and solvothermal techniques, ultrasound-induced methods ion-liquid, evaporation, thermal plasma and sol–gel processes [20–25].

In this study we used a mesoporous TiO_2 material, produced by sol–gel technique [26–28], to develop new carbonized-TiO_2 anode materials for lithium-ion batteries. Using a surfactant based technique; it is possible to transform directly a fraction of the carbon utilized in the synthesis process to produce C-nanocomposites having distributed carbon inside the pores and, at the same time, a very high specific surface. This porous matrix also offers unique advantages for further carbon impregnation processes.

In this work, we studied the nanostructural evolution of this mesoporous TiO_2 during the process of carbonization in a N_2 atmosphere up to 700 °C, the temperature normally needed for the synthesis of a semiconducting carbon layer [29]. The amount of carbon inside the pores was found to influence the final microstructure upon thermal annealing. The pursue of this work is the coat a special structure of TiO_2 and study the relation between the TiO_2 and the carbon, in particularly at high temperatures with

* Corresponding author. Tel.: +1 450 652 8019; fax: +1 450 652 8424.
E-mail address: zaghib.karim@ireq.ca (K. Zaghib).

0378-7753/$ – see front matter © 2011 Published by Elsevier B.V.
doi:10.1016/j.jpowsour.2011.11.029

the possibility that carbon may influence the titanium oxidation state.

2. Experimental procedure

The mesoporous powder was prepared following the details found in Ref. [28]. For the carbonization the mesoporous powder was impregnated in cellulose acetate. The powder was then heated at 400 °C for an hour and 700 °C for 3 h in a nitrogen atmosphere.

To understand the behavior of the microstructure and its evolution during carbonization process, the evolution of the mesoporous structure was studied, with and without prior impregnation by a carbon-based liquid at 400 °C during one hour in nitrogen atmosphere. The material was then heated at 700 °C for 3 h, also in a nitrogen atmosphere in order to synthesize a semiconducting carbon layer.

Materials were then studied by using different characterization techniques. Scanning electron microscope (SEM) observations were carried out with the S-4700 Hitachi SEM operated at the accelerating voltage of 5 kV. Conventional and high resolution transmission electron microscopy (TEM) investigations were made by using the high resolution dedicated STEM Hitachi HD-2700 operated at 200 kV, a HRTEM JEOL2100-F operated at 200 kV and a HRTEM Hitachi H-9000NA, operated at 300 kV. EELS analysis was done using a Gatan Enfina spectrometer in the HD-2700 STEM. In each case, the spectra were recorded for less than 1 min to present beam damage on the sample. The energy resolution in the present experimental conditions was about 0.4 eV.

X-ray diffraction spectra were obtained with a Bruker AXS D8 Advance diffractometer (using Cu Kα radiation) and the Raman spectra by using a microRaman HORIBA LabSpec 5 spectrometer (λ = 632.817 nm). Measurements of the percentage of carbon (wt%) were carried out with C/S detector from Leco and the BET (Brunauer–Emmett–Teller) specific surface areas were measured with a Quadrosorb SI Analyzer (Quantochrome Instrument).

The electrochemical discharge–charge characterization was performed by using a constant current method (MacPile®Claix, France).

3. Results

3.1. Microstructural investigation

Fig. 1a–c presents SEM images of the three different TiO_2 powders. As expected, thermal treatment in nitrogen (TT-N_2) up to 700 °C and the carbonization process caused a significant modification of the material structure. The sponge structure of the mesoporous material, showed in Fig. 1a, changed completely during the thermal treatment (Fig. 1b). Nanoparticles of about 10–30 nm are deposited onto larger faceplate clusters having dimensions of about 100–200 nm. Amorphous carbon is dispersed onto the surface of the clusters between and around the nanoparticles.

Carbonized material (TT-C—TiO_2) presents a similar structure of the treated one (TT-N_2) as it is shown in Fig. 1c. However in this case the amorphous carbon covers and wraps the nanoparticles.

Transmission electron microscopy investigations allowed to confirm the microstructural evolution of the material during the carbonization process and the thermal treatment. Fig. 2 presents the TEM images with the corresponding selected area electron diffractions (SAED) of the analyzed materials.

Annealing of the template materials at temperature around 150 °C allows the removal of the C, leading to the formation of a mesoporous amorphous structure [28]. Pores around 1–2 nm are visible in the amorphous TiO_2 clusters, as it is shown in Fig. 2a. The SAED in the Fig. 2b shows the typical signature of an amorphous phase. The BET specific surface area on the present powder was about 500 $m^2\ g^{-1}$. This value was found to vary over time because of the sensitivity of this material to air and humidity. Measurement of the carbon content revealed the presence of 5.5 wt% of carbon in the mesoporous powder, coming probably in large part from the original surfactant (the C content for the original powder was found to be around 25 wt%). However, since the powder was exposed to air, some amount of C can also come from adsorption of some carbon species.

During the thermal treatment in nitrogen (TT-N_2), the mesoporous TiO_2 crystallizes in two different phases, rutile and anatase, as it is possible to see in the selected area electron diffraction (SAED) in the Fig. 2d [25–30]. The SAED permits to identify the (1 0 1), (0 0 4) and (2 0 0) rings of the body-centered tetragonal anatase from nanoparticles of size between 10 and 50 nm, and the (1 1 0), (2 0 0) and (2 2 3) reflections of the tetragonal rutile phase from faceplate crystallites. From TEM, the rutile crystals have dimensions of about 150–250 nm. Amorphous carbon is dispersed between anatase particles onto the surface of rutile clusters. The amount of carbon is reduced to about 4 wt% because of the thermal treatment and its distribution is not homogeneous in the material. Because of the loss in porosity, the BET specific surface area is decreased to a value of about 75 $m^2\ g^{-1}$, significantly lower than in the original material.

The mesoporous TiO_2 sample, that was impregnated, presents a somewhat similar microstructure after the annealing process (TT-C—TiO_2), with the formation of rutile and anatase phases as it is possible to see in the Fig. 2e–f. Anatase TiO_2 particles, of dimensions between 10 and 50 nm, are again dispersed between well oriented rutile crystallites of more than 100 nm. All the particles have always polyhedral shape, typical of titanium oxide. The SAED is obtained from a region of about 100 nm large, as indicated by the white circle on the picture. The interpretation of the electron diffraction shows the same contribution seen in the TT-N_2 material with the typical rings of anatase nanoparticles and the reflections given from rutile planes. Some carbon specie is dispersed on the surface of the rutile clusters and covering and wrapping the anatase nanoparticles. Interestingly, the measured carbon concentration in this sample has nearly doubled to 7 wt%, as well as the value for the BET specific surface area at 128 $m^2\ g^{-1}$.

In Fig. 3a–c high resolution TEM images of the TT-TiO_2 and TiO_2—C-TT materials are presented respectively. In the first Fig. 3(a) a particle of anatase TiO_2 is shown and the {1 0 1} anatase lattice planes are identified (d{1 0 1} = 0.351 nm). Carbon is presented around the particle at the grain boundary.

In Fig. 3b the {1 0 1} lattice fringes of anatase phase are also visible in the carbonized sample. It is interesting to observe that anatase particles are immersed and enveloped in the amorphous carbon as results of impregnation process. Moreover some particles are agglomerated together inside the carbon. This fact explains the growth of the electron diffraction spots in the corresponding SAED (Fig. 2f) with respect to the electron diffraction in Fig. 2d. Fig. 3c shows the {1 1 0} lattice fringes of the rutile phase in a cluster (d = 0.327 nm). Carbon is observed on the surface of the cluster.

The carbon percentage (wt%) and the BET specific surface are reported in Fig. 4a for three different TiO_2 samples. The higher specific surface for the TT-C—TiO_2 can be attributed to a higher density of smaller anatase particles in this sample than in the previous one (TT-N_2). Carbon, impregnated in the mesoporous structure, would have a direct impact in the anatase grain growth because it could limit the transformation of the anatase structure into the rutile structure [31].

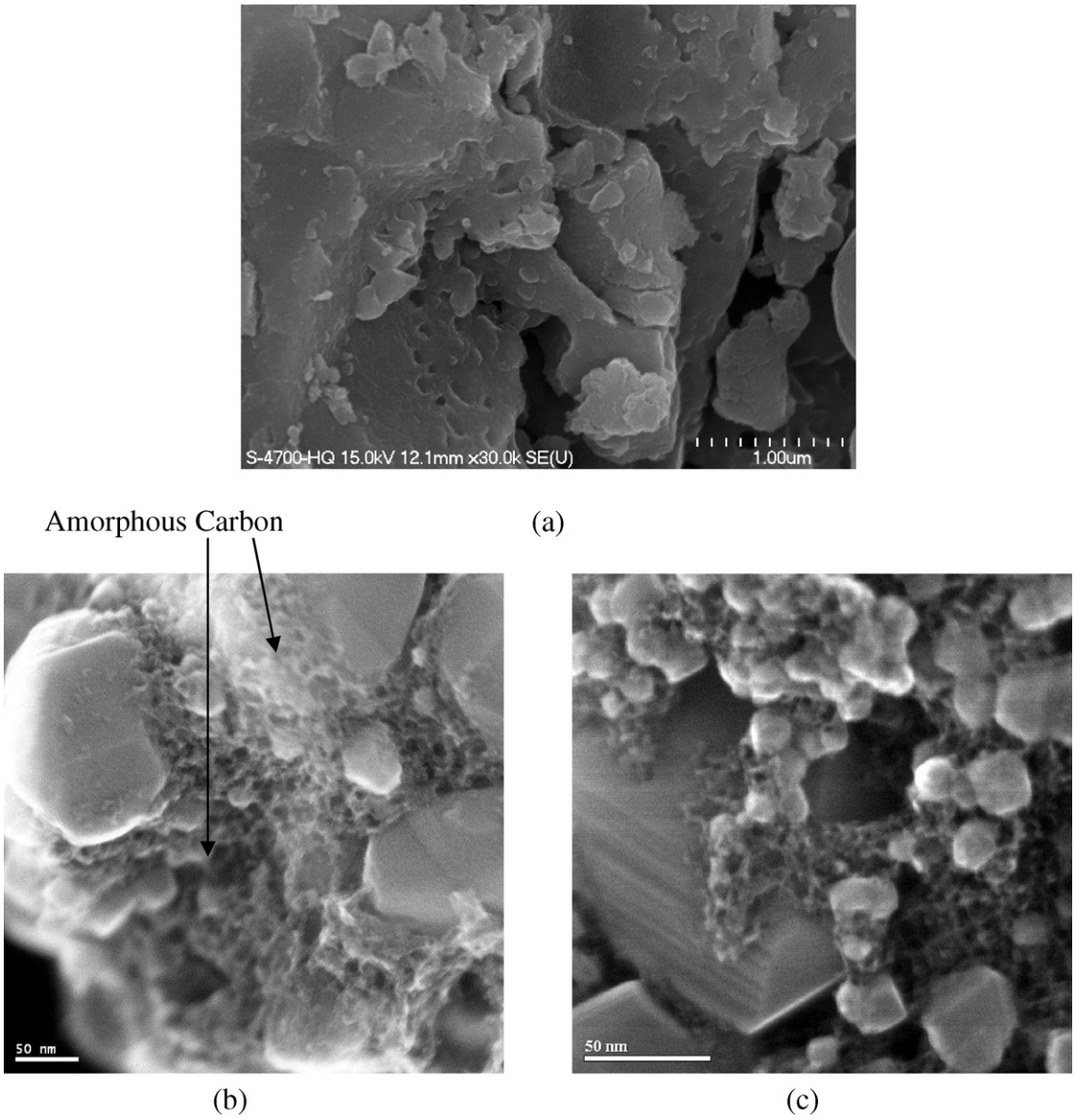

Fig. 1. SEM images of the mesoporous TiO_2 (a), of the material annealed at 400 °C for one hour and at 700 °C for 3 h in N_2 atmosphere (TT-N_2) and of the carbonized TiO_2 at 400 °C for one hour and annealed at 700 °C for 3 h in nitrogen (C—TiO_2-TT). The amorphous carbon is presented in the (b) between the nanoparticles, as indicated on the picture, and it covers the nanoparticles in (c).

The XRD spectra of materials are shown in Fig. 4b. The typical signature of an amorphous material is visible in the XRD spectrum given from the original mesoporous powder. For the other two materials the presence of rutile and anatase phases are detected. In the carbon impregnated material the signature of anatase is stronger then in the TT-N_2 sample confirming the higher concentration of anatase small grains observed in STEM. Again a higher density of smaller grains explains the higher value of the specific surface.

To confirm the reduction of grain size, we performed Rietvel analysis on the X-ray spectra for both crystalline materials. These simulations confirmed a reduction of grain size due to the C impregnation. The average rutile crystal size obtained was found to be ~70 nm in the TT-N_2 sample compared to ~40 nm for the TT-C—TiO_2, while the anatase average size was reduced from 12–20 nm to 5.3–10 nm. The difference between these X-ray results and the TEM observation could be due to differences in sampling between the two methods.

Fig. 4c presents the Raman spectra of the three samples. The interpretation of the Raman spectrum is not evident for the mesoporous sample; it clearly shows the presence of organic compounds in the material coming from the recipe used to produce the template and the mesoporous material [23]

Rutile and anatase contributions are well identified for the others materials and the two picks typical of a disordered carbon structure [32] are easily visible between 1200 and 1700 cm^{-1}.

Fig. 4d presents the Ti EELS core loss spectra for the mesoporous sample and also for the rutile and anatase nanocrystals found in the TT-C—TiO_2 sample. For the rutile and anatase nanocrystals, one observes the variation in the different peak intensity typical of these two structures in agreement with the recent paper by Cheynet et al. [33]. For the starting mesoporous sample, one notes a larger FWHM for all the different energy contributions, probably due to the largely amorphous nature of this material. However, the relative intensity of the different energy contributions tends to suggest

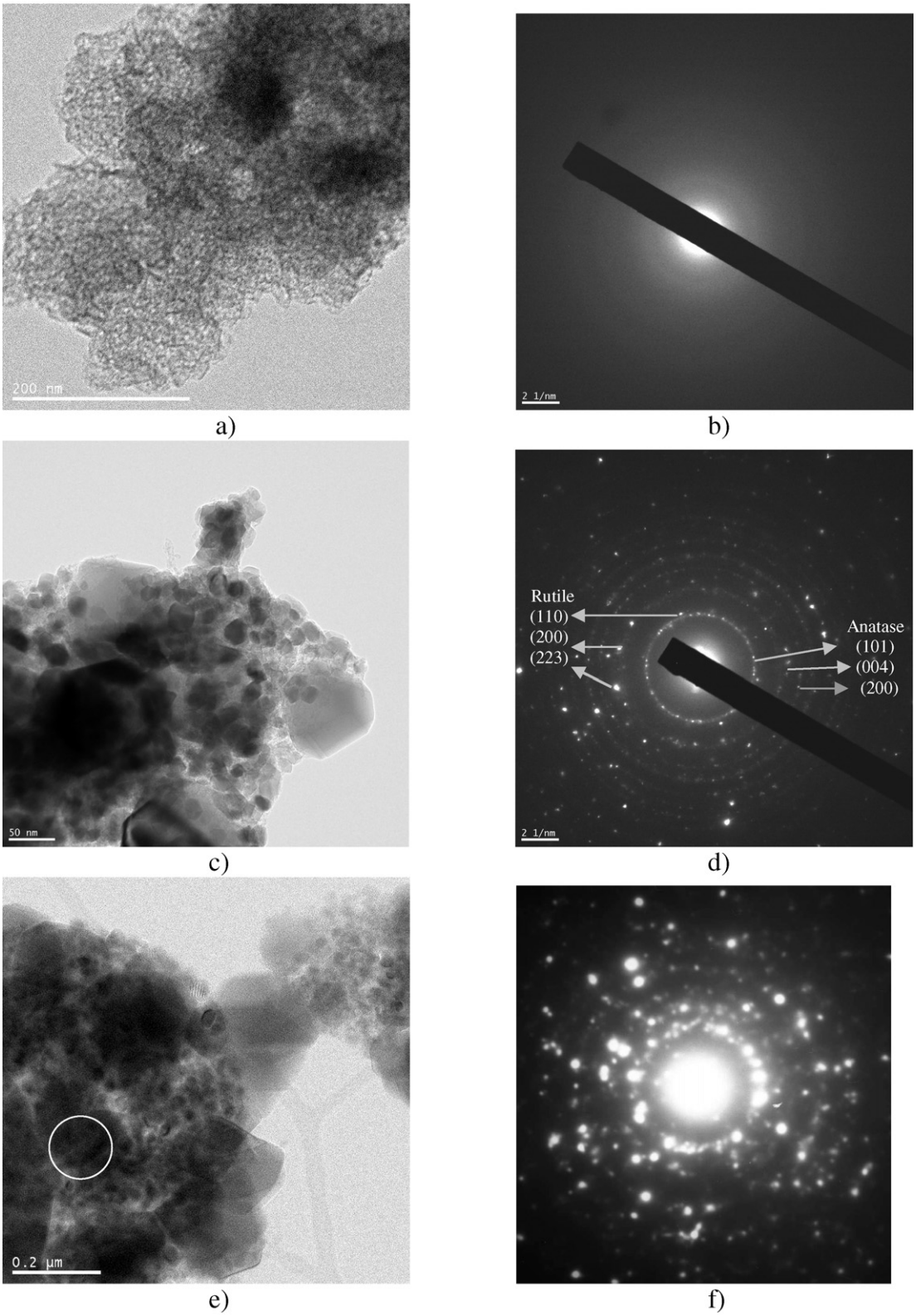

Fig. 2. (a and b) TEM image of the mesoporous TiO_2 material and the corresponding SAED showing the typical signature of amorphous TiO_2; (c and d) STEM images in transmission mode of the TT-N_2 TiO_2 material with its SAED showing the contributions of both anatase and rutile phases; (e and f) STEM images in transmission mode of the TT-C—TiO_2 sample and the SAED from the circled region in (f).

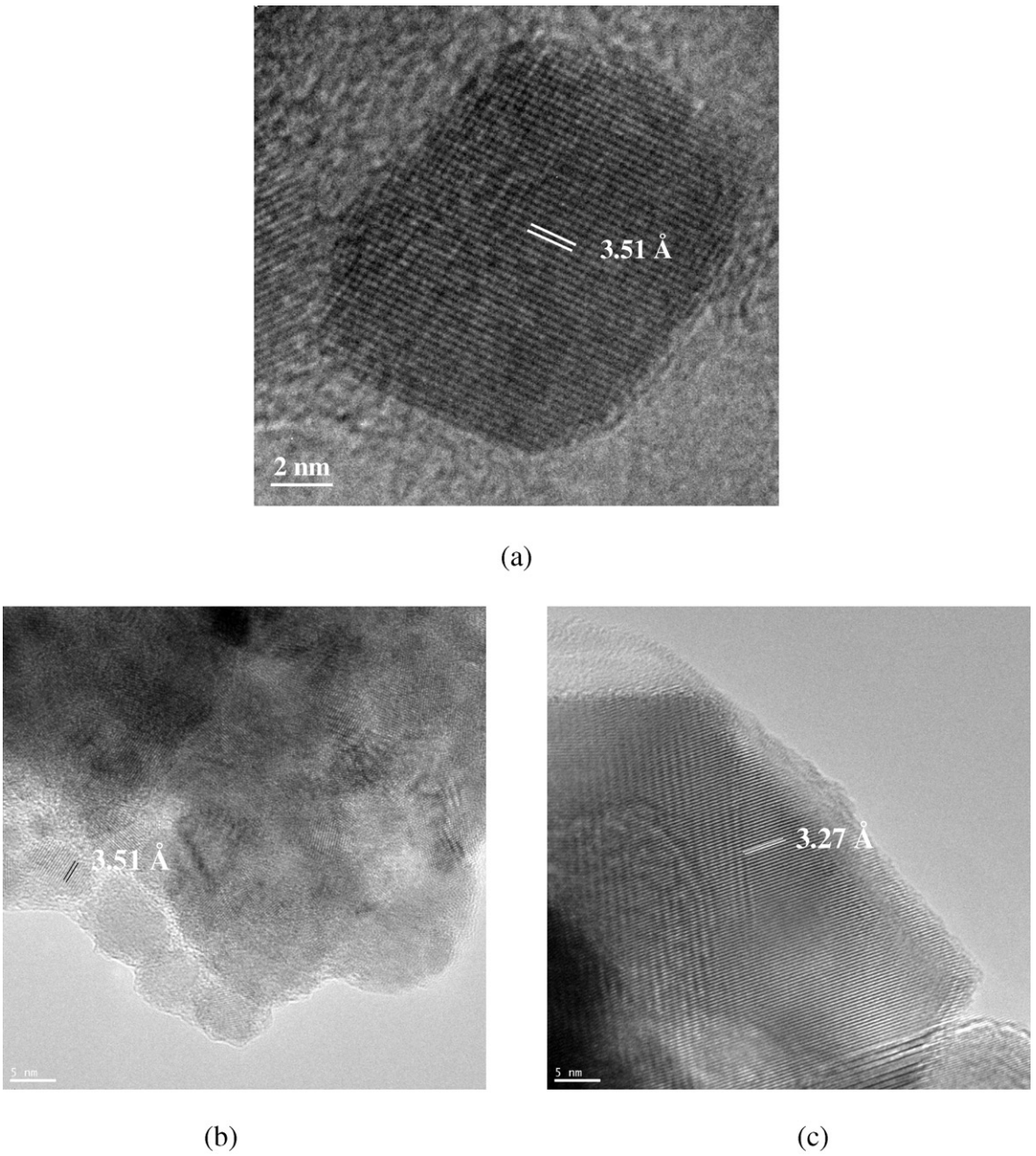

Fig. 3. (a) High resolution TEM image of a particle of anatase phase in the TT-N_2 sample: the {1 0 1} anatase TiO_2 lattice planes are identified; (b) lattice TEM image of a region of the carbonized material: anatase particles, with the 1 0 1 lattice fringes, are immersed and enveloped in the amorphous carbon; (c) in the same specimen the {1 1 0} lattice fringes of the rutile phase are visible in the clusters. Amorphous carbon is presented at the surface of the clusters.

that the structural nature is more related to anatase than rutile in this sample.

3.2. Electrochemical behavior

The electrochemical performance of these various TiO_2 materials was analyzed in half-cells with lithium (TiO_2/Li). The discharge–charge profiles of the first cycles are shown in Fig. 5 for the mesoporous and carbonized TiO_2 samples. The applied current rate is C/24 (about 0.24 mA g^{-1}) over a potential window of 1.2–2.5 V. For the mesoporous material, the capacity obtained in the first cycle is 150 mAh g^{-1} with a coulomb efficiency of 71% in the first cycle and 90% in the second cycle. In the second cycle we observed a decrease in the reversible capacity to 115 mAh g^{-1}. The loss of reversibility is probably due to the formation of a solid electrolyte interface (SEI) that is not unusual in this kind of materials [34]. The current rate was then increased to 1 C (about 5 mA g^{-1}). Fig. 6 shows the profile of the 20th cycle obtained within this rate. Several cycles are performed with good capacity retention, but the capacity is reduced to 110 mA g^{-1}.

4. Discussion and conclusions

In general, one would expect a better electrochemical capacity of the anode material after complete carbonization once the electronic conductivity is enhanced [35]. Interstitial carbon acts as a doping element in the crystal TiO_2 lattice and the carbon coating increases the electrical conductivity of material [36]. However, in the present case it is interesting to observe that the carbonized sample showed a lower capacity compared to the mesoporous

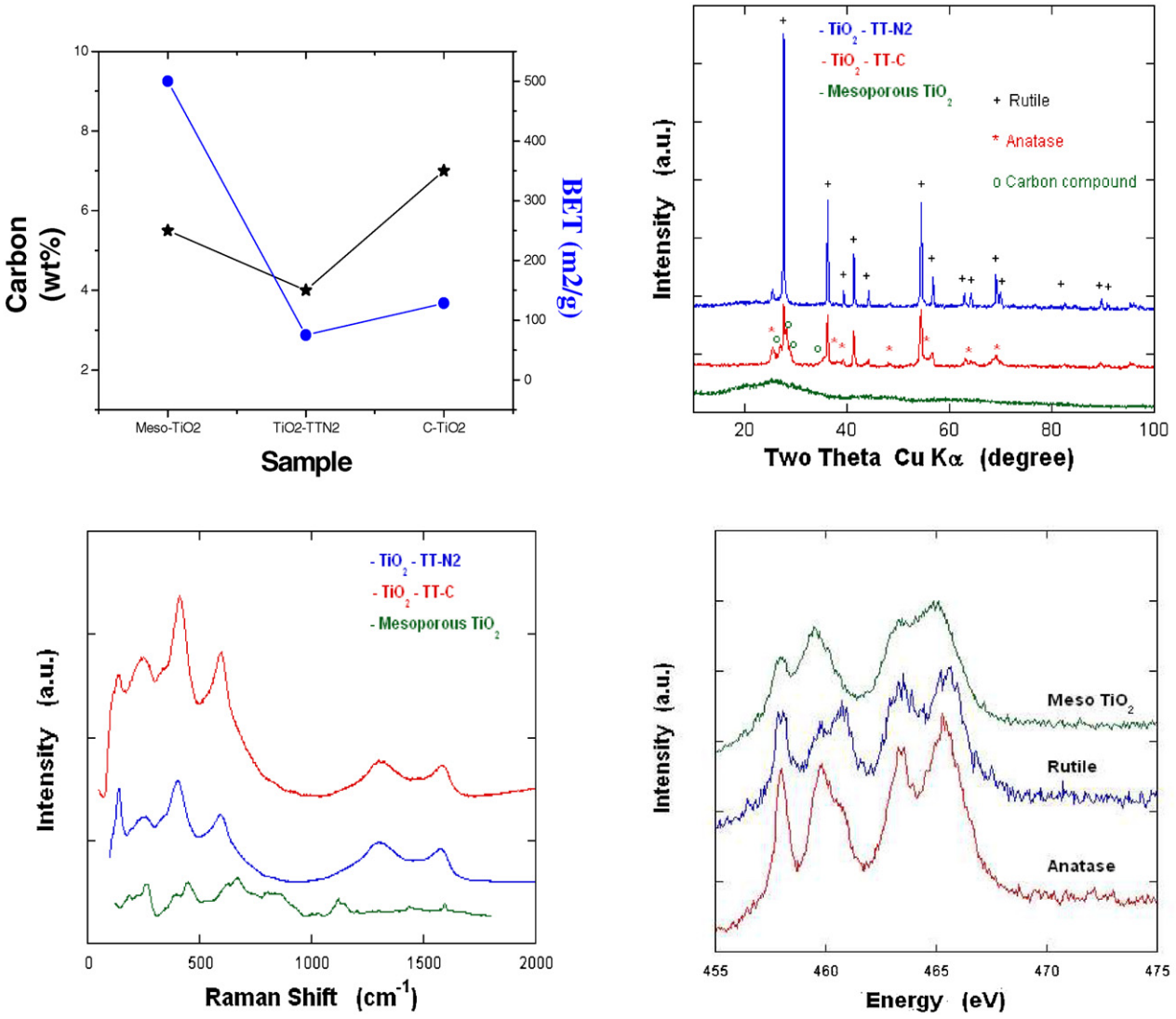

Fig. 4. (a) Behavior of the carbon percentage (wt%) and of the BET surface specific ($m^2\ g^{-1}$) in the three TiO_2 samples (TT = thermal treatment); (b) XRD spectra in which it is evident the amorphous signature of the original material and the strong presence of the rutile phase after the annealing and the carbonization processes; (c) Raman spectra (λ = 632.817 nm) obtained from the three TiO_2 specimens; and (d) Ti EELS core-loss spectra for the mesoporous sample and for the anatase and rutile nanocrystals.

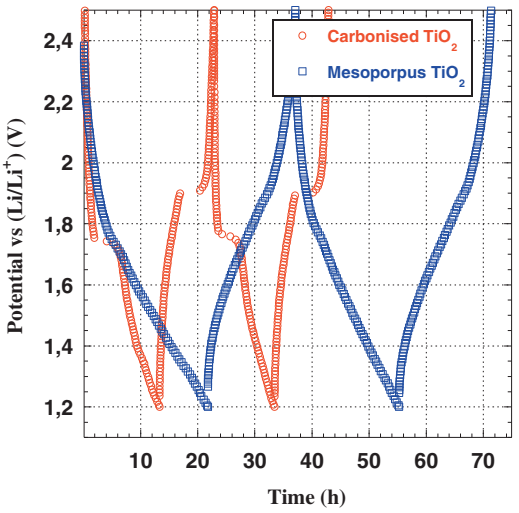

Fig. 5. The galvanostatic discharge–charge profiles of the half-cell TiO_2/Li at a current rate of C/24.

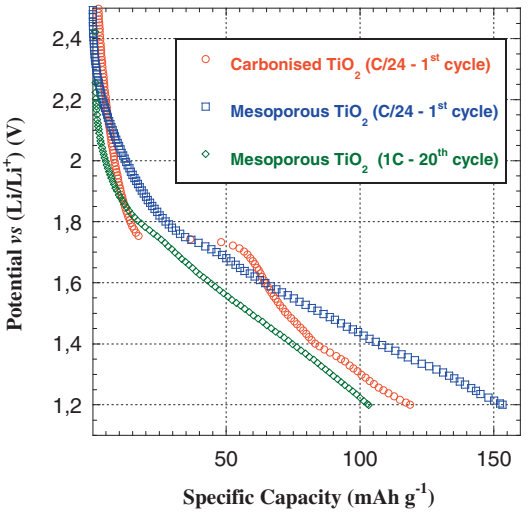

Fig. 6. The discharge profiles of TiO_2/Li half-cells at C/24 and 1 C rate.

material. In effect the carbonization process and, above all, the thermal treatment needed for this carbonization, caused a too strong modification of the nanostructure of the original mesoporous TiO_2. The material has lost completely its original mesoporosity, and the nucleation and growth of two crystalline phases has happen. This microstructural evolution limits the specific surface and then is detrimental to the electrochemical behavior of the TiO_2 anode.

We thus developed mesoporous and nanostructured TiO_2 anodes with very high specific surface, up to more than 500 $m^2\ g^{-1}$, that show good promise for lithium battery applications. Modifying the surfactant to form a carbon coating inside the pores at low temperature shows better promises than normal carbonization processes, since the high temperature needed is too high and results in the crystal formation and the loss of porosity.

In future works we will analyze different processing conditions of the surfactant by varying the temperature of the thermal treatments. The goal is to produce a conductive carbon coating inside the pores or a highly porous carbon coated anatase nanoparticles with very high specific surface area.

Acknowledgements

We thank René Veillette for the technical support and the useful discussion during SEM, TEM and Raman analysis. We thank also Patrick Charest and Marie Claude Mathieu for the specimen preparation, Julie Trottier and Martin Dontigny for the electrochemical tests.

References

[1] R.W. Siegel, Nanostructured Materials 3 (1993) 1.
[2] H. Gleiter, Nanostructured Materials 1 (1992) 1.
[3] J.Y. Ying, Chemical Engineering Science 61 (2006) 1540.
[4] A. Fujishima, T.N. Rao, D.A. Tryk, Journal of Photochemistry and Photobiology C: Photochemistry Reviews 1 (2000) 1.
[5] S.M. Oh, S.S. Kim, J.E. Lee, T. Ishigaki, D.W. Park, Thin Solid Films 435 (1–2) (2003) 252.
[6] Y. Hwu, Y.D. Yao, N.F. Cheng, C.Y. Tung, H.M. Lin, Nanostructured Materials 9 (1–8) (1997) 355–358.
[7] Z. Yang, D. Choi, S. Kerisit, K. Rosso, D. Wang, J. Zhang, G. Graff, J. Liu, Journal of Power Sources 192 (2) (15 July 2009) 588–598.
[8] V.G. Pol, S.H. Kang, J.M. Calderon-Moreno, C.S. Johnson, M.M. Tackeray, Journal of Power Sources 195 (2010), 5039.
[9] H. Qiao, L. Xiao, L. Zhang, Electrochemistry Communications 10 (2008), 616.
[10] M. Mancini, P. Kubiak, J. Geserick, R. Marassi, N. Husing, M. Wohlfahrt-Mehrens, Journal of Power Sources 189 (1) (2009) 585–589.
[11] B. Erjavec, R. Dominko, P. Umek, S. Sturm, A. Pintar, M. Gaberscek, Journal of Power Sources 189 (1) (1 April 2009) 869–874.
[12] L.J. Fu, L.C. Yang, Y. Shi, B. Wang, Y.P. Wu, Microporous and Mesoporous Materials 117 (2009) 515.
[13] S. Yoon, B.H. Ka, C. Lee, M. Park, S.M. Oh, Electrochemical and Solid-State Letters 12 (2) (2009) A28.
[14] L.J. Fu, T. Zhang, Q. Cao, H.P. Zhang, Y.P. Wu, Electrochemistry Communications 9 (2007) 2140.
[15] H. Qiao, L. Xiao, L. Zhang, Electrochemistry Communications 10 (2008) 616.
[16] Y. Shen, J. Tao, F. Gu, L. Huang, J. Bao, J. Zhang, N. Dai, Journal of Alloys and Compounds 474 (1–2) (17 April 2009) 326–329.
[17] T. An, J. Liu, G. Li, S. Zhang, H. Zhao, X. Zeng, G. Sheng, J. Fu, Applied Catalysis A: General 350 (2) (30 November 2008) 237–243.
[18] T.V. Gestel, D. Sebold, W.A. Meuenberg, Bram S M., H.-P. Buchkremer, Solid State Ionics 179 (2008) 1360.
[19] H.-G. Jung, S.W. Oh, J. Ce, N. Jayaprakash, Y.-K. Sun, Electrochemistry Communications 11 (2009) 756–759.
[20] S.-M. Oh, T. Ishigaki, Thin Solid Films 457 (2004) 186.
[21] Y. Chen, S. Lunsford, D.D. Dionysiou, Thin Solid Films 516 (2008) 7930.
[22] C.-C. Chang, C.-K. Lin, C.-C. Chan, C.-S. Hsu, C.-Y. Chen, Thin Solid Films 494 (2006) 274.
[23] C.A. Chen, K.Y. Chen, Y.S. Huang, D.S. Tsai, K.K. Tiong, F.Z. Chien, Journal of Crystal Growth 310 (2008) 3663.
[24] H.-D. Jang, H. Chang, K. Cho, S.-J. Kim, J.-H. Park, J.-W. Choi, K. Okuyama, Ultramicroscopy 108 (2008) 1241.
[25] Y. Guo, K. Ono, N. Murata, T. Okazaki, Journal of Crystal Growth 275 (2005) e2031.
[26] D.M. Antonelli, J.Y. Ying, Mesoporous Materials. Current Opinions in Colloid and Interface Science 1 (1996) 523.
[27] P. Kubiak, J. Geserick, N. Husing, M. Wohlfahrt-Mehrens, Journal of Power Sources 175 (2008) 510.
[28] D.M. Antonelli, J.Y. Ying, Angewandte Chemie, International Edition in English 34, No. 18, 1995, p. 2014.
[29] B. Erjavec, R. Dominko, P. Umek, S. Sturm, A. Pintar, M. Gaberscek, Journal of Power Sources 189 (2009) 869.
[30] L. Zhao, M. Han, J. Lian, Thin Solid Films 516 (2008) 3394.
[31] T. Tsumura, N. Kojitani, H. Umemura, M. Toyoda, M. Inagaki, Applied Surface Science 196 (2002) 429–436.
[32] M.S. Dresselhaus, G. Dresselhaus, K. Sugihara, I.L. Spain, H.A. Goldberg, in: U. Gonser, A. Mooradian, K.A. MÜller, M.B. Panish, H. Sakaki (Eds.), Graphite Fibers and Filaments, Springer Series in Materials Science 5, 1988, pp. 98–103.
[33] M. Cheynet, S. Pokrant, S. Irsen, P. Krüger, Ultramicroscopy 110 (2010) 1046.
[34] Y.-H. Jin, S.-H. Lee, H.-W. Shim, K.-H. Ko, D.-W. Kim, Electrochemical Acta 55 (2010) 7315.
[35] U. Lafont, L. Simonin, M. Gaberscek, E.M. Kelder, Journal of Power Sources 174 (2007) 1104–1108.
[36] C. Chen, M. Long, H. Zeng, W. Cai, B. Zhou, J. Zhang, Y. Wu, D. Ding, D. Wu, Journal of Molecular Catalysis A: Chemical 314 (2009) 35–41.